Data in Brief 59 (2025) 111414

Contents lists available at ScienceDirect

Data in Brief

journal homepage: www.elsevier.com/locate/dib

Data Article

Data of the crystal structure of xylose isomerase from *Streptomyces avermitilis*

Ki Hyun Nam

College of General Education, Kookmin University, Seoul 02707, Republic of Korea

ARTICLE INFO

Article history:
Received 11 October 2024
Revised 14 February 2025
Accepted 17 February 2025
Available online 21 February 2025

Dataset link: Crystal structure of Xylose isomerase from Streptomyces avermitilis (Original data).
Dataset link: X-ray diffraction data of xylose isomerase from Streptomyces avermitilis (Original data).

Keywords:
Xylose isomerase
Glucose isomerase
X-ray diffraction data
Crystal structure
Metal binding site

ABSTRACT

Xylose isomerase (XI; also known as glucose isomerase) catalyzes the conversion of D-glucose and D-xylose to D-fructose and D-xylulose, respectively. XI is widely used in various industries, such as high-fructose corn syrup and bioethanol production. The discovery and characterization of novel XI variants are important to enhance the effective industrial applications of XI. Recently, the X-ray diffraction data for XI from *Streptomyces avermitilis* (SavXI) were collected at a synchrotron. The crystal structure of SavXI was determined using the molecular replacement method. The SavXI structure exhibited two unique metal-binding sites at the active site, diverse conformations, and a distinctive conformation of the C-terminal region compared to other XI homologs. This structural information extends the understanding of the molecular properties of the XI family. Here, information on the raw diffraction data images of SavXI, which were not presented in the previous study, is introduced. Detailed data collection and structure determination are reported for future XI structural analyses.

E-mail address: structure@kookmin.ac.kr

https://doi.org/10.1016/j.dib.2025.111414

Specifications Table

Subject	Biological sciences
Specific subject area	Structural Biology
Type of data	Raw data, Processed
Data collection	Experiment type: X-ray diffraction Synchrotron source: Pohang Light Source II (PLS-II, Pohang, Republic of Korea) Beamline: 7A (Structural Biology I) X-ray wavelength: 0.9793 Å (monochromatic) X-ray exposure time: 100 ms / image (1° rotation) Detector: Quantum 270 CCD detector (ADSC, Poway, CA, USA). Data collection temperature: 100 K Intensity-integration software: HKL2000 (HKL Research, Inc., Charlottesville, VA, USA) Data scaling software: HKL2000 (HKL Research, Inc., Charlottesville, VA, USA)
Data source location	Institution: Kookmin University City/Town/Region: Seoul Country: Republic of Korea
Data accessibility	X-ray Diffraction images Repository name: Zenodo (https://zenodo.org) Data identification number: http://doi.org/10.5281/zenodo.13841141 Direct URL to data: https://zenodo.org/records/13841141 Structure factor and coordinate Repository name: Protein Data Bank (http://rcsb.org) Data identification number: https://doi.org/10.2210/pdb8YUD/pdb Direct URL to data: https://www.rcsb.org/structure/8YUD Instructions for accessing these data: X-ray diffraction images and structure factor/coordinates can be downloaded from the above website without permission.
Related research article	Nam, K.H. Structural Analysis of Xylose Isomerase from *Streptomyces avermitilis*. Crystals 2024, 14(5), 446; https://doi.org/10.3390/cryst14050446 [1]

1. Value of the Data

- The X-ray diffraction images of the crystal structure of SavXI were provided.
- The structure factors and coordinates of the crystal structure of SavXI were reported.
- The diverse conformations of the metal-binding site at the active site and a unique conformation of the C-terminal α-helix domain of SavXI were compared with other XI family members.
- These data provide insights into XI engineering to enhance enzyme activity for industrial applications.

2. Background

Xylose isomerase (XI; also known as glucose isomerase) is an aldose isomerase that converts sugar molecules [2,3]. The ability of XI to convert D-glucose to D-fructose is widely applied in the food industry for producing high-fructose corn syrup [4–6]. The conversion of D-xylose to D-xylulose by XI is also utilized in the biorefinery industry for bioethanol production [7–9]. To improve the enzymatic activity of XI for industrial applications, protein engineering and the discovery of new XI variants are ongoing [10]. Understanding its structural properties is important for efficient industrial utilization and rational engineering of XI [11–13]. To provide structural information for protein engineering, the crystal structure of a novel XI from *Streptomyces avermitilis* (SavXI) has recently been determined [1]. This SavXI structure reveals unique structural properties of the metal-binding site involved in the isomerization reaction and the C-terminal domain involved in the stable oligomeric state of XI. This structural information is useful for

understanding the molecular properties of the XI family. In the previous study, details of the data collection process and the quality of the final model structure were not reported. Additionally, information on the raw diffraction images of SavXI was not included but is provided in this study. To provide insights for subsequent research on the XI structure, detailed data collection, data quality, and unique structural information on SavXI are reported here.

3. Data Description

X-ray diffraction (XRD) data of SavXI were collected using cryocrystallography techniques at beamline 7A at the Pohang Light Source II (PLS-II; Pohang, Republic of Korea). The SavXI crystal was soaked in a cryoprotectant solution and exposed to X-rays on the goniometer at 100 K in the experimental hutch. A single SavXI crystal was exposed to X-rays for 360 s during a 360° rotation, resulting in 360 XRD images. These raw XRD data of SavXI were deposited on Zenodo (DOI:10.5281/zenodo.13841141). Detailed data collection information, including X-ray parameters and detector, is listed in Table 1.

The original XRD data for SavXI were processed using the HKL2000 program. SavXI crystals were indexed as belonging to the trigonal space group $P3_221$. Image processing results indicated that 150 images (image nos. 110–249) exhibited relatively high quality with low R-factor values compared to the other images. To generate a higher-quality dataset, only these 150 images were processed and used to determine the crystal structure of SavXI. In a previous report, although only 150 images were used, additional XRD images could be included in a further reanalysis to improve the completeness of the dataset. The statistics for XRD images processed using these 150 images are summarized in Table 2.

The SavXI crystal belongs to the trigonal space group $P3_212$, with unit cell dimensions of a = b = 129.13 Å, c = 233.05 Å, $\alpha = \beta = 90°$, and $\gamma = 120°$. The Matthews coefficient value is 2.18 Å^3/Da, with a solvent content of 43.58%, indicating that six SavXI molecules exist in the asymmetric unit. Data processing results showed that the overall completeness, I/σ, R_{merge}, R_{pim}, CC1/2, and CC* were 97.8%, 11.24, 0.262, 0.107, 0.977, and 0.994, respectively. In the low-resolution region (50–7.59 Å), the completeness, I/σ, R_{merge}, R_{pim}, CC1/2, and CC* were 99.1%, 45.20, 0.075, 0.030, 0.996, and 0.999, respectively (Fig. 1). In the high-resolution region (2.85–2.80 Å), the completeness, I/σ, R_{merge}, R_{pim}, CC1/2, and CC* were 97.5%, 2.10, 1.260, 0.506, 0.627, and 0.878, respectively (Fig. 1). Based on these data statistics, the structural determination of SavXI at a resolution better than 2.8 Å is feasible in the further reanalysis of this dataset.

Table 1
Parameters of oscillation data processing.

Parameter	Value
Wavelength (A)	0.97933
Raster size (mm)	0.12956
Raster size (mm)	0.12956
Film width (mm)	270.00
Film length (mm)	270.00
Record length (pixels)	2084
Number of records	2084
spots rejected when pixel overflow at value	65500.0
Detector to crystal distance	348.64
X beam	134.70
Y beam	138.20
Beam polarization	0.99000
Indexing parameter*	
Horizontal box size	4.6641
Vertical box size	4.6641

* This parameter can vary depending on the processing methods used by the researcher, and the values mentioned here are those utilized in the previous data processing.

Table 2
Data collection statistics of SavXI.

Data collection	SavXI		
Space group	$P3_221$		
Cell dimension			
a, b, c (Å)	129.13, 129.13, 233.05		
α, β, γ (°)	90.00, 90.00, 120.00		
Matthews coefficient (Å³/Da)	2.18		
solvent content (%)	43.58		
Resolution (Å)	50.0-2.80	50.0-7.59	2.85-2.80
Unique reflections	54119	2964	2664
Completeness (%)	97.8	99.1	97.5
Redundancy	6.4	7.1	6.4
I/σ	11.24	45.2	2.1
R_{merge}	0.262	0.075	1.260
R_{meas}	0.284	0.081	1.360
R_{pim}	0.107	0.030	0.506
CC1/2	0.977	0.996	0.627
CC*	0.994	0.999	0.878

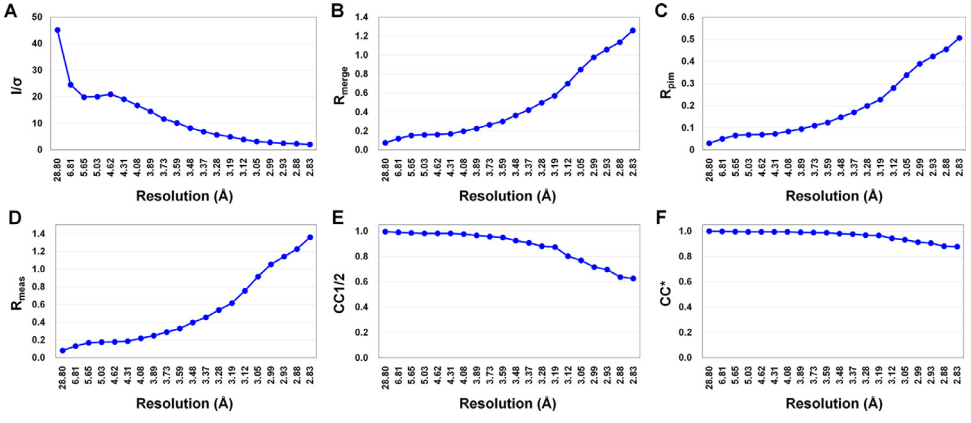

Fig. 1. Statistics of data processing for XRD data of SavXI. Data processing plots of SavXI using 150 images (image nos. 100–149) for (A) I/σ, (B) R_{merge}, (C) R_{pim}, (D) R_{meas}, (E) CC1/2, and (F) CC*.

The phase problem of the processed data for SavXI was solved using molecular replacement with the MOLREP program and default parameters. The crystal structure was determined at a resolution of 2.80 Å, with R_{work} and R_{free} values of 0.187 and 0.243, respectively. The root mean square (r.m.s.) deviations for bonds and angles were 0.009 Å and 1.136°, respectively. The detailed structure determination statistics for SavXI are summarized in Table 3.

A total of 2304 amino acids were built from the six SavXI molecules in the asymmetric unit. The geometry of the final model of the SavXI structure was evaluated using a Ramachandran plot (Fig. 2). Of the residues, 2181 (94.66%) were positioned in the favored region, whereas 110 (4.77%) were in the allowed region. Thirteen (0.56%) residues were in the disallowed region. The following residues were identified as outliers: Glu186 ($\varphi°$, $\psi° = 70.6, 119.3$) and Phe357 (−165.6, −89.1) from chain A; Pro7 (−46.6, −12.7), Glu186 (45.2, 110.9), and Phe357 (−162.2, −85.5) from chain B; Glu186 (68.8, 108.0) and Phe357 (−154.8, −96.3) from chain C; Glu186 (66.0, 114.3) and Tyr280 (−60.7, 95.8) from chain D; Pro184 (−87.6, −36.3) and Glu186 (61.8, 119.9) from chain E; and Glu186 (62.8, 115.9) and Asn247 (−171.1, −145.6) from chain F. A more detailed geometry analysis of the final model structure of SavXI is listed in Table 4.

The crystal structure of SavXI consists of an N-terminal TIM-barrel fold containing the active site and a C-terminal α-helical domain involved in stabilizing the tetrameric formation of XI.

Table 3
Statistics of the structure refinement of SavXI.

Refinement	SavXI
Resolution (Å)	34.21-2.80
MIN (Fobs/SIGMA_Fobs)	1.330
Completeness (%)	97.5
R value (Working + TEST set)	0.189
R value (Working set)	0.187
Free R value	0.243
Error estimates (Maximum-likelihood based)	
Coordinate error	0.380
Phase error (degrees)	23.56
R.m.s. deviations	
Bonds (Å)	0.009
Angles (°)	1.136
B factors (Å^2)	
Protein	35.87
Metal ion	36.99
Ramachandran plot	
Favored (%)	94.66
Allowed (%)	4.77
Disallowed (%)	0.56
PDB code	8YUD

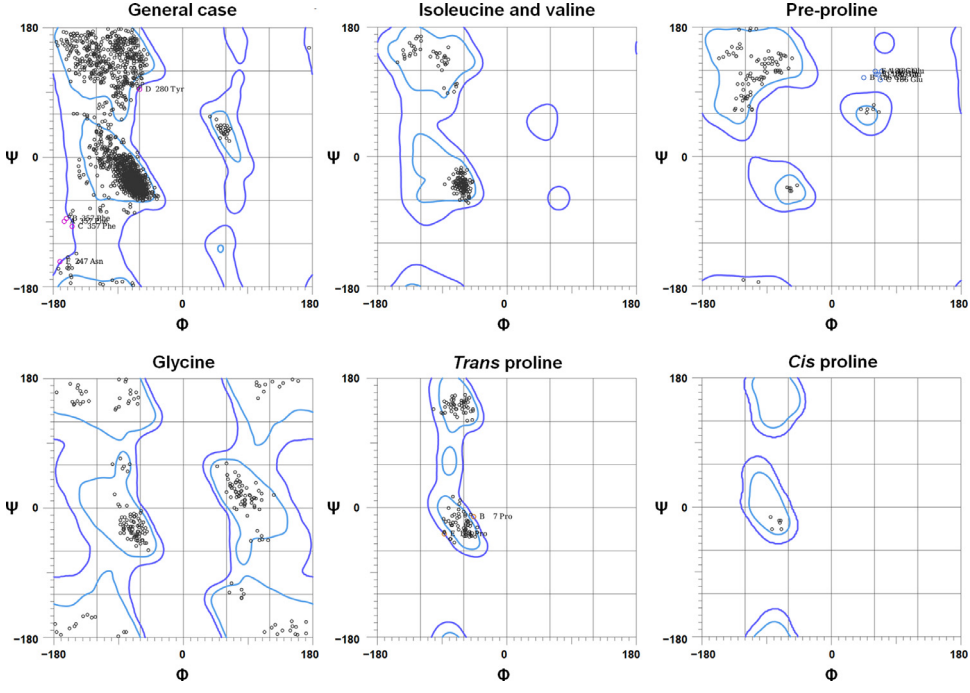

Fig. 2. Ramachandran plot for the final model structure of SavXI (PDB code 8YUD). The circles indicate the distribution of backbone dihedral angles (ϕ, ψ) of residues in the SavXI structure. Residues in the outlier regions are marked by red circles, with the residue name and number.

Table 4
Summary detailed geometry statistics of SavXI.

		Residue number	Percentage (%)
Protein Geometry	Poor rotamers	52	2.92
	Favored rotamers	1433	80.42
	Ramachandran outliers	13	0.56%
	Ramachandran favored	2181	94.66%
	Rama distribution Z-score	-3.69 ± 0.14	
	Cβ deviations >0.25Å	0	0.00%
	Bad bonds:	0 / 18504	0.00%
	Bad angles:	3 / 25086	0.00%
Peptide Omegas	Cis Prolines:	6/114	5.26%
Low resolution Criteria	CaBLAM outliers	34	1.5%
	CA Geometry outliers	12	0.52%
Additional validations	Chiral volume outliers	0/2646	0

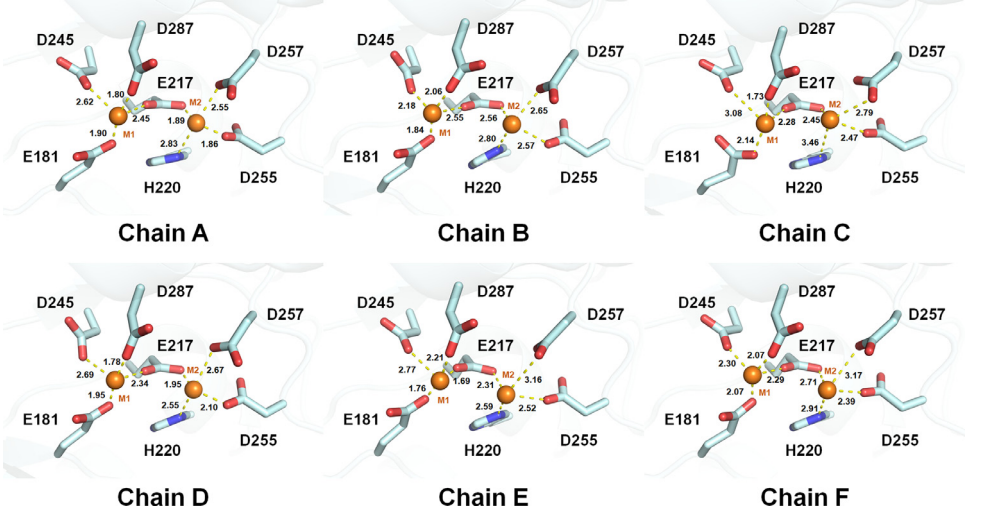

Fig. 3. Metal-binding sites at the active site of SavXI. Six SavXI molecules in the asymmetric unit exhibit diverse metal ion binding configurations. The interactions between the metal ions and residues are indicated by yellow dotted lines.

This monomeric SavXI further forms a tetrameric structure. In the asymmetric unit, four SavXI molecules create a tetrameric arrangement with 222 noncrystallographic symmetries. Two more SavXI molecules form a tetrameric configuration with others in symmetric positions within the crystal lattice. The analysis of the tetrameric interface of SavXI has been reported in a previous study [1]. The metal-binding sites and the conformations of these sites differ slightly among the six molecules (Fig. 3). Detailed structural analysis regarding the interactions between the metal ions and their coordinating residues, coordination angles for metal-binding sites in SavXI, and the unique conformation of the C-terminal α-helical domain have been analyzed and compared in a previous study [1].

This study provides detailed information on data collection and structure determination. The original XRD data (raw data, totaling 360 images for 360° rotation) have been deposited in Zenodo. These XRD images (img format) contain header information regarding data collection, such as X-ray and detector specifications. Reprocessing of XRD images can be performed using crystallographic programs such as HKL2000 or Mosflm. The final model structure (pdb or cif format) and structure factors (mtz format) of the SavXI structure have been deposited in the PDB. Other data collection and structure determination information has also been registered on the PDB site. These raw and processed data can be downloaded without permission.

4. Experimental Design, Materials and Methods

Protein preparation and crystallography experimental procedures were reported in a previous study [1]. The recombinant DNA containing the gene encoding XI from *S. avermitilis* (UniProt: Q93HF3), with an N-terminal thrombin cleavage site, was transformed into *Escherichia coli* BL21 (DE3) cells. Cells were grown in LB medium with 50 μg/mL ampicillin at 37°C until the OD_{600} reached 0.8. Recombinant SavXI protein expression was induced with 0.5 mM isopropyl β-D-1-thiogalactopyranoside and further incubated in a shaking incubator at 18°C overnight. After harvesting cells by centrifugation at 4000 rpm for 30 min, the cell pellet was lysed in a lysis buffer containing 50 mM Tris-HCl (pH 8.0) and 200 mM NaCl by sonication. After removing cell debris by centrifugation at 13,000 rpm for 1 h, the supernatant was purified by Ni-NTA affinity chromatography. The eluted protein was incubated with thrombin protease to remove the N-terminal expression tag, including hexahistidine. The protein was concentrated using a centricon (Merck Millipore, Burlington, MA, USA; cutoff: 30 kDa) and loaded onto gel filtration chromatography using a HiPrep 16/60 Sephacryl S-200 HR column (GE Healthcare, Chicago, IL, USA). The purified protein was in a buffer containing 10 mM Tris-HCl (pH 8.0) and 200 mM NaCl and was concentrated using a centricon (Merck Millipore, Burlington, MA, USA; cutoff: 30 kDa) to ~30 mg/mL for crystallization. Crystallization experiments were performed using the sitting drop vapor diffusion method at 20°C. Suitable orthorhombic SavXI crystals for XRD were grown under crystallization conditions containing 0.1 M Tris-HCl (pH 8.5) and 8% (w/v) polyethylene glycol 8000. XRD data collection was performed at beamline 7A at Pohang Light Source II (PLS-II, Pohang, Republic of Korea) [14]. The SavXI crystal was cryoprotected using a crystallization solution supplemented with 25% (v/v) ethylene glycol for 5 s. XRD data were collected at 100 K under a nitrogen gas stream. XRD data were indexed, integrated, and scaled using HKL2000 [15]. The electron density map was obtained using the molecular replacement method with the MOLREP (version 11.2.08) [16] program implemented in CCP4 suite [17] using the crystal structure of glucose isomerase from *Streptomyces rubiginosus* (PDB code 7DFJ) [12] as the search model. Manual model building was performed with COOT (version 0.9.6) [18]. Structure refinement was conducted using phenix.refine in PHENIX (version 1.20.1_4487) [19]. Water molecules were automatically added using default parameters during structure refinement. The geometry of the final model structure was validated using MolProbity server (http://molprobity.biochem.duke.edu/) [20].

Limitations

During protein preparation and crystallization, metal ions were not added to the purified SavXI. Consequently, the type of metal ions in the active site of SavXI was not identified. The occupancy of the metal ions at the active site was also not determined.

Ethics statement

This work meets the ethical requirements for publication in this journal. This work does not involve human subjects, animal experiments, or any data collected from social media.

Credit author statement

Ki Hyun Nam: Data curation, Formal analysis, Validation, Visualization, Writing – original draft, Funding acquisition.

Data availability

Crystal structure of Xylose isomerase from Streptomyces avermitilis (Original data). (Protein Data Bank).
X-ray diffraction data of xylose isomerase from Streptomyces avermitilis (Original data). (ZENODO).

Acknowledgements

The author acknowledges support at beamline 7A, Pohang Accelerator Laboratory, Pohang, South Korea. This work was funded by the National Research Foundation of Korea (NRF) (NRF-2021R1I1A1A01050838). The author thanks the Global Science experimental Data Hub Center (GSDC) at the Korea Institute of Science and Technology Information (KISTI) for providing computing resources and technical support.

Declaration of competing interests

The authors declare that they have no known competing financial interests or personal relationships that could have appeared to influence the work reported in this paper.

References

[1] K.H. Nam, Structural Analysis of Xylose Isomerase from Streptomyces avermitilis, Crystals 14 (5) (2024) 446, doi:10.3390/cryst14050446.
[2] S.H. Bhosale, M.B. Rao, V.V. Deshpande, Molecular and industrial aspects of glucose isomerase, Microbiol. Rev. 60 (2) (1996) 280–300, doi:10.1128/mr.60.2.280-300.1996.
[3] K.H. Nam, Glucose isomerase: functions, structures, and applications, Appl. Sci. 12 (1) (2022) 428, doi:10.3390/app12010428.
[4] L.Q. Jin, Q. Xu, Z.Q. Liu, D.X. Jia, C.J. Liao, D.S. Chen, Y.G. Zheng, Immobilization of recombinant glucose isomerase for efficient production of high fructose corn syrup, Appl. Biochem. Biotechnol. 183 (1) (2017) 293–306, doi:10.1007/s12010-017-2445-0.
[5] K. Visuri, A.M. Klibanov, Enzymatic production of high fructose corn syrup (HFCS) containing 55% fructose in aqueous ethanol, Biotechnol. Bioeng. 30 (7) (2004) 917–920, doi:10.1002/bit.260300715.
[6] J.S. White, Straight talk about high-fructose corn syrup: what it is and what it ain't, Am. J. Clin. Nutr. 88 (6) (2008) 1716S–1721S, doi:10.3945/ajcn.2008.25825B.
[7] H. Alper, G. Stephanopoulos, Engineering for biofuels: exploiting innate microbial capacity or importing biosynthetic potential? Nat. Rev. Microbiol. 7 (10) (2009) 715–723, doi:10.1038/nrmicro2186.
[8] J.H. Van Vleet, T.W. Jeffries, Yeast metabolic engineering for hemicellulosic ethanol production, Curr. Opin. Biotechnol. 20 (3) (2009) 300–306, doi:10.1016/j.copbio.2009.06.001.
[9] R. Domingues, M. Bondar, I. Palolo, O. Queirós, C.D. de Almeida, M.T. Cesário, Xylose metabolism in bacteria—opportunities and challenges towards efficient lignocellulosic biomass-based biorefineries, Appl. Sci. 11 (17) (2021) 8112, doi:10.3390/app11178112.
[10] K.H. Nam, Engineering xylose isomerase for industrial applications, Catalysts 14 (9) (2024) 597, doi:10.3390/catal14090597.
[11] K.H. Nam, Crystal structure of the metal-free state of glucose isomerase reveals its minimal open configuration for metal binding, Biochem. Biophys. Res. Commun. 547 (2021) 69–74, doi:10.1016/j.bbrc.2021.02.026.
[12] K.H. Nam, Room-temperature structure of xylitol-bound glucose isomerase by serial crystallography: xylitol binding in the M1 site induces release of metal bound in the M2 site, Int. J. Mol. Sci. 22 (8) (2021) 3892, doi:10.3390/ijms22083892.
[13] Y. Xu, K.H. Nam, Xylitol binding to the M1 site of glucose isomerase induces a conformational change in the substrate binding channel, Biochem. Biophys. Res. Commun. 682 (2023) 21–26, doi:10.1016/j.bbrc.2023.09.087.
[14] S.Y. Park, S.C. Ha, Y.G. Kim, The protein crystallography beamlines at the pohang light source II, Biodesign 5 (1) (2017) 30–34.
[15] Z. Otwinowski, W. Minor, Processing of X-ray diffraction data collected in oscillation mode, Methods Enzymol 276 (1997) 307–326, doi:10.1016/S0076-6879(97)76066-X.
[16] A. Vagin, A. Teplyakov, Molecular replacement with MOLREP, Acta Crystallogr. D Biol. Crystallogr. 66 (Pt 1) (2010) 22–25, doi:10.1107/S0907444909042589.

[17] J. Agirre, M. Atanasova, H. Bagdonas, C.B. Ballard, A. Baslé, J. Beilsten-Edmands, R.J. Borges, D.G. Brown, J.J. Burgos-Mármol, J.M. Berrisford, P.S. Bond, I. Caballero, L. Catapano, G. Chojnowski, A.G. Cook, K.D. Cowtan, T.I. Croll, J.É. Debreczeni, N.E. Devenish, E.J. Dodson, T.R. Drevon, P. Emsley, G. Evans, P.R. Evans, M. Fando, J. Foadi, L. Fuentes-Montero, E.F. Garman, M. Gerstel, R.J. Gildea, K. Hatti, M.L. Hekkelman, P. Heuser, S.W. Hoh, M.A. Hough, H.T. Jenkins, E. Jiménez, R.P. Joosten, R.M. Keegan, N. Keep, E.B. Krissinel, P. Kolenko, O. Kovalevskiy, V.S. Lamzin, D.M. Lawson, A.A. Lebedev, A.G.W. Leslie, B. Lohkamp, F. Long, M. Malý, A.J. McCoy, S.J. McNicholas, A. Medina, C. Millán, J.W. Murray, G.N. Murshudov, R.A. Nicholls, M.E.M. Noble, R. Oeffner, N.S. Pannu, J.M. Parkhurst, N. Pearce, J. Pereira, A. Perrakis, H.R. Powell, R.J. Read, D.J. Rigden, W. Rochira, M. Sammito, F. Sánchez Rodríguez, G.M. Sheldrick, K.L. Shelley, F. Simkovic, A.J. Simpkin, P. Skubak, E. Sobolev, R.A. Steiner, K. Stevenson, I. Tews, J.M.H. Thomas, A. Thorn, J.T. Valls, V. Uski, I. Usón, A. Vagin, S. Velankar, M. Vollmar, H. Walden, D. Waterman, K.S. Wilson, M.D. Winn, G. Winter, M. Wojdyr, K. Yamashita, The CCP4 suite: integrative software for macromolecular crystallography, Acta Crystallogr. D Struct. Biol. 79 (6) (2023) 449–461, doi:10.1107/s2059798323003595.

[18] A. Casañal, B. Lohkamp, P. Emsley, Current developments in coot for macromolecular model building of electron cryo-microscopy and crystallographic data, Protein Sci. 29 (4) (2020) 1055–1064, doi:10.1002/pro.3791.

[19] D. Liebschner, P.V. Afonine, M.L. Baker, G. Bunkoczi, V.B. Chen, T.I. Croll, B. Hintze, L.W. Hung, S. Jain, A.J. McCoy, N.W. Moriarty, R.D. Oeffner, B.K. Poon, M.G. Prisant, R.J. Read, J.S. Richardson, D.C. Richardson, M.D. Sammito, O.V. Sobolev, D.H. Stockwell, T.C. Terwilliger, A.G. Urzhumtsev, L.L. Videau, C.J. Williams, P.D. Adams, Macromolecular structure determination using X-rays, neutrons and electrons: recent developments in Phenix, Acta Crystallogr. D Struct. Biol. 75 (Pt 10) (2019) 861–877, doi:10.1107/S2059798319011471.

[20] C.J. Williams, J.J. Headd, N.W. Moriarty, M.G. Prisant, L.L. Videau, L.N. Deis, V. Verma, D.A. Keedy, B.J. Hintze, V.B. Chen, S. Jain, S.M. Lewis, W.B. Arendall 3rd, J. Snoeyink, P.D. Adams, S.C. Lovell, J.S. Richardson, D.C. Richardson, MolProbity: more and better reference data for improved all-atom structure validation, Protein Sci 27 (1) (2018) 293–315, doi:10.1002/pro.3330.